Self-consistent dynamics of wall slip

Self-consistent dynamics of wall slip

Johan L.A. Dubbeldam and Jaap Molenaar
Faculty of Mathematics and Computer Science,
Technische Universiteit Eindhoven, Den Dolech 2,
5600 MB Eindhoven, The Netherlands,
jdubbeld@win.tue.nl, phone: +31-40-247-2685 fax: +31-40-247-2685
(Dated: January 9, 2002)

We studied the entanglement-disentanglement transition in order to explain wall slip in a polymer melt. We consider a tube model for tethered chains in which the most important relaxation mechanisms, convective constraint release and chain stretching/retraction, are incorporated and we take the interactions between tethered chains and bulk flow self-consistently into account.

Numerical simulations show that our model exhibits an entanglement-disentanglement transition, leading to a jump in the slip velocity which increases with the number of entanglements and the grafting density. The wall shear stress is found to be a non-monotonic function of the slip velocity and the shear rate, yielding the possibility of hysteresis and spurt instabilities. Our analysis reveals the existence of a dimensionless parameter which determines the time scale of the dynamics for the slowing down of the melt. The relative rate at which relaxation of the tethered chain and slowing down of the melt take place, seems to be quintessential for the slip behavior of the melt.

I. INTRODUCTION

The so-called no-slip boundary condition has been scrutinized since a long time. Molecular dynamics simulations [1] and experiments have shown that for Newtonian fluids the no-slip condition is in general satisfied. However, for polymer flows (melts) it has been known for many years that slip may occur if a polymer melt flows along a solid surface [2]. In 1979 de Gennes [3] demonstrated that slippage in polymer flows is due to the high viscosity of polymer fluids.

The goal of this paper is to provide a physical picture of wall slip for the case in which the slip is caused by disentanglement of chains grafted on the wall from the polymers in the bulk. We will restrict ourselves to polymer melts, for these are of most interest for practical purposes. If long polymer chains are grafted on the solid interface, the slip is greatly reduced, but does not disappear [4]. It was realised that the mechanism governing the transition from stick to slip boundary conditions could be found in an entanglement-disentanglement transition. This mechanism predicts that there are essentially three different slip regimes [3, 4].

In the first regime the velocity near the wall is very small, so that the tethered molecule will entangle with the flow and has a more or less random spherical configuration. The friction between the tethered molecule and the melt will be Stokes-like, that is, it is proportional to the radius of gyration of the attached molecule which depends linearly on the square root of the polymerization index N. The wall shear stress increases first linearly, but always monotonicly with the velocity near the wall, which can be identified with the (wall) slip velocity. When the slip velocity increases beyond a certain value, we enter the second regime in which the tethered molecule has no longer a spherical shape, but is stretched to a degree at which the friction scales linearly with N, so-called Rouse friction. Since this friction force is much weaker than the Stokes friction, the molecule retracts, after which it will stretch again. This breathing regime is referred to as the *marginal regime*. The breathing implies that the time-averaged stress is constant for a range of velocities [27]. When the velocity near the wall increases still more, we reach the third regime in which the tethered molecule is completely disentangled from the melt and almost permanently in a stretched state so that the friction is Rouse-like. In the third regime the stress near the wall increases again monotonicly with the slip velocity.

If instead of the flow velocity near the wall, the shear stress is considered as the independent quantity one finds the following. When the wall shear stress is very small, there will be a negligible slip velocity. This slip velocity increases monotonicly with shear stress, until a critical value of the shear stress is reached. When the stress is increased beyond this value a large increase in the slip velocity is observed, after which the slip velocity will again increase slowly with wall shear stress.

The theory behind the mechanism of slip and some modified versions thereof [4–6] have been experimentally confirmed in Refs. [7–9]. In these papers the wall slip velocity has been directly measured in the vicinity of the wall. It displays a transition from low slip to high slip as a function of the apparent shear rate. However, for grafting densities for which the theory of Ref. [3] should apply, the transition measured is less steep than predicted [9]. Only for grafting densities more than ten to hundred times higher than the critical grafting density, a steep transition from no-slip to slip is observed.

In most experiments evidence of slip is indirect. In an extrusion experiment as sketched in Fig. 1, the throughput is measured as a function of the pressure difference

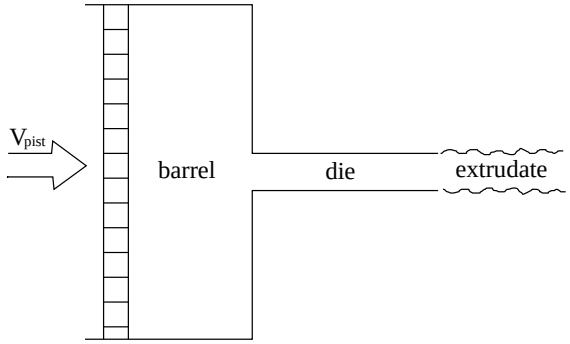

FIG. 1: A sketch of the set up for an extrusion experiment. The wave like perturbations in the extrudate indicate spurt oscillations.

or visa versa. Increasing the pressure, which amounts to increasing the wall shear stress, gives rise to (surface) instabilities, such as *sharkskin*, *spurt*, and *gross melt fracture*. Keeping the piston speed constant leads to sharkskin for low piston speeds and to gross melt fracture when the piston is very high. The pressure shows an intermediate regime of large oscillations, usually denoted by spurt. Sharkskin indicates small surface distortions and gross melt fracture is commonly used for large distortions which not merely affect the surface, but also the volume of the extrudate. In Refs. [10, 11] it was demonstrated qualitatively that some of these instabilities may originate from a phase transition. Their description in terms of Ginzburg-Landau theory requires a non-monotonic relation between the slip velocity and the wall shear stress, which was simply assumed. Here we show how the slip velocity versus shear stress relation depends on the molecular parameters, and that a non-monotonic relation between shear stress and slip velocity can actually occur.

Although the entanglement-disentanglement phenomenon gives a good qualitative description of the fact that polymer systems exhibit a nonzero slip velocity at the wall, the time dependent dynamics of the transition is usually not considered. Theories that do describe the dynamics of polymeric fluids are reptation theories in which stresses are calculated for a prescribed shear rate. In stick-slip situations the flow is not constant in time, but changes due to entanglements between tethered and bulk chains, which suggests that one cannot use a prescribed shear rate description. One way to overcome these difficulties is to separate the flow region into two parts: a layer near the wall, the so-called interfacial layer, and a bulk layer which comprises all the polymers which do not belong to the interfacial layer. This method has been pursued in Ref. [12], and gives results which agree rather well with experiments.

Here we follow a complementary approach based on the full dynamics of the grafted chains, which takes the influence of the grafted chains on the bulk flow into account in a self-consistent way. This means that we have to consider both the dragging force of the bulk on the grafted chains and the action of the grafted molecules on the flow (velocity) of the polymers in the bulk. For the movement of the grafted chains we need to invoke molecular theories describing entangled polymer systems. Here we apply a modified version of the Doi-Edwards theory that was put forward by Mead, Larson and Doi [13] and which describes entangled polymers which can reptate, retract, stretch and show contour length fluctuations. Furthermore, the relaxation mechanism which is important for intermediate times, the so-called convective constraint release (CCR) mechanism, was taken into account. The model was dubbed contour variable model and consists of a set of partial differential equations for the stress tensor, the length and orientation of the polymers. Very recently this contour variable model has been applied to model wall slip [12]. Since we are interested in the stick-slip transition and the physical mechanism behind it, we concentrate on the dynamics of the grafted chains and their interactions with the bulk. We therefore solve the equations of motion of the grafted chains numerically, which amounts to solving a system of stochastic differential equations. This approach of handling polymer flows was also applied in Ref. [14]. Our description contains all ingredients that were also present in Refs. [12, 13], but it additionally provides us with a clear physical picture behind the slip mechanism.

The entanglements between tethered and bulk chains give rise to constraints for the tethered chains. These constraints are depicted as points, which form a grid through which the tethered chain cannot pass. The entangled grafted chain finds its way by performing a random walk, caused by thermal fluctuations and interactions with the bulk molecules. We remark that the rate of entanglement between grafted and non-grafted molecules is determined by two competing mechanisms.

1. The bulk molecules passing by tend to squeeze the grafted chains against the wall. If the chains would not be subject to random forces, the chains would just align with the flow and in their final equilibrium state the molecules would all be maximally stretched and lying along the wall.

2. Since there are Brownian forces the chains are continuously changing there conformation, thereby creating new or annihilating existing entanglements with the bulk polymers. These volatile conformational changes are often called contour length fluctuations when the fluctuations are small, or breathing modes, when the tube is really renewed.

So we may summarize as follows. In our model the interactions between the bulk molecules in the flow and the the grafted chains are accounted for in a self-consistent way, that is, the velocity profile of the bulk molecules is slowed down due to entanglements between grafted and bulk chains and simultaneously the attached polymer chains are dragged along with the flow. This will lead to a

velocity profile in which two regions can be distinguished. In the layer near the wall, the interfacial layer, the velocity rapidly decreases, whereas in the remaining region, the bulk region, the shear rate is constant. A similar division in two layers was also performed in Ref. [12], but there the thickness of the boundary layer did not depend on the shear rate, but was simply a parameter. Here we calculate the thickness of the interfacial layer and the velocity profile within this layer self-consistently, which shows that they depend on the shear rate.

We should further stress that the model does not require the slip velocity to be prescribed. The slip velocity is actually calculated self-consistently as the velocity of that layer of the bulk polymers near the wall, which is the first layer not entangled with the grafted chains in the interfacial layer. The slip velocity is shown to depend on the upper plate velocity in plane Couette flow and a few molecular parameters. We observe that the velocity exhibits a jump as a function of the plate velocity, which is more pronounced when the polymerization index N of the grafted chains increases. We also find that the onset of slip increases with the the grafting density ν, approximately linearly, which was also predicted in Ref. [5] and confirmed experimentally.

Moreover, the relation between stress and slip velocity is shown to be a non-monotonic function. An ingredient which, when coupled to the momentum equation for the bulk flow, can give rise to all kind of instabilities like spurt and sharkskin [10].

This paper is divided into four sections. In the next section we will give a detailed description of the model. The numerical results are presented in section III and the conclusions and discussion are given in section IV.

II. DESCRIPTION OF THE MODEL

We study the molecular chain dynamics very close to the lower plate of a plane Couette flow; see Fig. 2. For simplicity we assume in our model that the motion of a tethered chain is restricted to the plane defined by the flow of the bulk for reasons of computational efficiency. Extension of the numerical simulations to three-dimensional dynamics of the tethered chain is not believed to alter our results qualitatively or to yield additional insight.

In our description we start from a tube on a two-dimensional grid. Initially the grid is square with a lattice parameter a. The grid represents the topological constraints which are imposed on the movement of the tethered polymer chains by the bulk molecules. The grid points are assumed to move in layers parallel to the wall. When a layer moves, it is assumed that all grid points in the layer move with the same velocity, which implies that the distance between two neighboring grid points in the same layer, is equal to a for all times. Different layers will have different velocities, since the grafted chains will slow down the movement of the grid whenever they are in contact with the grid. The interaction between the grid and the grafted chains takes places at localized points where the grid points and the grafted chains touch; these points are called entanglements. Since the number of entanglements increases when the distances to the wall decreases, the velocity is rapidly decreasing in the vicinity of the wall.

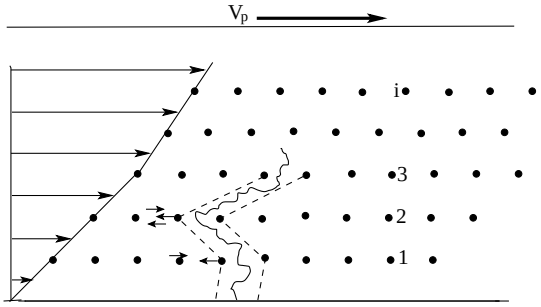

FIG. 2: Sketch of the flow of the grid of constraints. Due to interactions between the grafted chains and the bulk molecules, the velocity is smallest near the wall. In the self-consistent approach not only the interactions of the bulk polymers on the grafted chains are taken into account, but also the reaction of the bulk. The interactions between grafted chains and bulk molecules are local at the entanglement points. This achieves a similar restricted movement of the tethered chain as the depicted tube.

The chains which are attached to the wall, commonly referred to as grafted or tethered chains, have to find their way through the grid. If one connects the grid points between which the grafted chain moves, one obtains the tube from Doi-Edwards theory, as is depicted in Fig. 2. Between two neighboring grid points in the same layer, we imagine a small ring through which the tethered chain may pass; this ring is called a slip link, following [20–22] and the chain can move frictionless through it.

The flow and thus the grid is moving under influence of a shear force exerted by moving the upper plate. At the upper plate we assume that the no-slip boundary condition applies. The bulk-wall interaction is studied in detail near the lower plate. Although our results are derived for the case of Couette flow, a generalization to the -for extrusion more common- Poiseuille flow is straightforward. Our preference for Couette flow is mainly because it facilitates comparison with experimental results which are primarily available for the case of Couette flow [7–9]. Furthermore, the dynamics very close to the wall is not susceptible to the flow properties far away.

The grafted chains are supposed to be homogeneously distributed along the wall with density ν. The interactions between different grafted chains is neglected, which implies that the grafting concentration is sufficiently low, i.e. $\nu R_0^2 < 1$, where R_0 denotes the radius of gyration of the grafted chains. This regime is often referred to as the mushroom regime. Later on we shall apply the model also for higher grafting densities, since experiments sug-

gest that the interaction between grafted chains can still be neglected, for densities up to more than ten times the critical density $\nu_c = \frac{1}{R_0^2}$.

The tethered chains are described by bead-spring or Rouse chains. They move through the grid points and only interact with the slip links through which they pass; see also Fig. 3. Due to the interaction with the convecting bulk, the tethered chains will stretch. The Brownian motion tends to redistribute the beads, so that the beads are distributed uniformly over the chain [22]. This Brownian motion, leading to redistribution of the beads between the slip links, constitutes the fastest relaxation process. Next the tube starts to attain its equilibrium length. This happens at a larger time-scale, usually identified with the Rouse time. Finally, at a still larger time-scale, the tube starts to reorientate, that means that the chain leaves its original tube and forms a new tube, so that the stress is relaxed. It is this reorientation or tube renewal which is most important for the entanglement-disentanglement transition. It can be caused by several mechanisms. When one does not deal with grafted chains and the shear rate is small, the dominating process responsible for reorientation of the tube is reptation. For high shear rates convective constraint release (CCR) becomes important [13].

Since we are dealing with grafted chains, reptation cannot occur and stress has to be relaxed by arm retraction or breathing of the chains. Besides this relaxation mechanism, the chain can relax by constraint release. In this process constraints disappear due to reptation of the bulk chains. Therefore the constraints actually have a finite lifetime, which is of the order of the reptation time of the bulk chains. Since this process is not important for the stick slip transition, especially in the case of short tethered chain [6], but merely introduces extra slip for low plate velocities, we shall not take it into account in our calculations. The most important relaxation mechanism that is involved in the transition from stick to slip is CCR. It describes the convection of constraints due to the movement of the grid of entanglements and a non-affine deformation of the grafted chains [13]. Particularly at high shear rates this process becomes important and determines the relaxation time of the tethered chains. So, for tube renewal we have two relaxation mechanisms: CCR which is dominant at high plate velocities, and arm retraction for low plate velocities.

Since the length of the attached chains is finite, there can only be entanglements between grafted and bulk chains in a region near the wall with thickness of the order of the gyration radius of the tethered molecules. The average thickness of this interfacial layer depends on the velocity (or shear rate) near the wall. That is why we do not prescribe the thickness of the boundary. Similarly we do not assume the slip velocity to be given as in Refs.[4, 5], but we define the slip velocity as the time averaged velocity of the grid layer on the boundary of the interfacial and bulk regions. The precise value of the slip velocity is not susceptible to the choice of the grid layer; as long as the chosen layer is not too far from the wall and part of the bulk flow, the velocity is practically equal to the slip velocity.

After this general description of the model we will now focus on the evolution equations for the polymers in the melt and the grafted chains.

A. Dynamics of the tethered chains

The assumption that the grafted chains are two-dimensional Gaussian chains implies that the beads obey the Langevin equations

$$\zeta_1 \frac{\partial \mathbf{x}_n}{\partial t} = \frac{3k_BT}{b^2}\left[\mathbf{x}_{n+1}(t) + \mathbf{x}_{n-1}(t) - 2\mathbf{x}_n(t)\right] + \mathbf{f}_n(t), \quad (1)$$

where ζ_1 is the friction coefficient of a monomer, $\mathbf{x}_n(t)$ describes the position of the n-th bead, b denotes the Kuhn length and $\mathbf{f}_n(t)$ is a Langevin force. The components of the Gaussian random force $f_n^i(t)$ satisfy

$$< f_n^i(t) >= 0, \quad < f^i{}_n(t_1) f_m^j(t_2) >= 2k_BT\zeta_1\delta(t_1 - t_2)\delta_{nm}\delta_{ij},$$

where i, j stand for x or y.

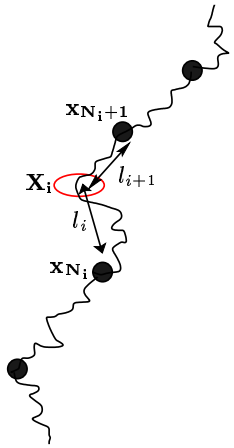

FIG. 3: Detail of the configuration of the chain in a tube. The interaction between the bead after the slip link and the bead just before the slip link are calculated from the tension in the chain passing through the slip link.

Of course, Eqs. (1) are only valid when there are no constraints. The constraints constituted by the grid points are modelled by slip links. The slip links involved constitute a tube like region, as depicted in Fig. 3. Since the bulk chains and hence the rings are moving, the tube consisting of slip links is changing its shape in time. The chain inside the tube will adapt in its turn to the new shape of the tube and hence changes its conformation. The interaction between the grafted polymers and the bulk is only local, namely at the the positions of the slip links. The movement of the grid is felt by the rest of the chain indirectly, namely through their interactions with

the neighboring beads. This implies that the Eqs.(1) are only valid for the beads not adjacent to a slip link (or to the wall). We denote the beads after which we have a slip link by N_1, $N_2, \cdots N_{N_{\rm seg}}$. For these beads, that are adjacent to a slip link, we have the following equation of motion

$$\zeta_1 \frac{\partial \mathbf{x}_{N_i}}{\partial t} = \frac{3k_BT}{b^2}\Big[-2\mathbf{x}_{N_i} + \mathbf{x}_{N_i-1} + \mathbf{X}_i(t) + \frac{l_{i+1}}{l_i}(\mathbf{X}_i(t) - \mathbf{x}_{N_i})\Big] + \mathbf{f}_{N_i}(t), \quad i = 1, \cdots, N_{\rm seg}, \tag{2}$$

where l_i and l_{i+1} are the lengths of the chain segments connecting bead N_i and the ring and the length of the chain connecting the ring and the N_i + 1-th bead, respectively. The slip link coordinate is denoted by $\mathbf{X}_i(t)$. A similar equation holds for the beads that are adjacent from above to a sliplink, having positions $\mathbf{x}_{N_1+1}(t), \mathbf{x}_{N_2+1}, \cdots, \mathbf{x}_{N_{\rm seg}+1}$; see also Fig. 3.

If we non-dimensionalize our equations and use as unit of length the Kuhn length b and as unit of time τ_1, which is defined by

$$\tau_1 = \frac{b^2\zeta_1}{3k_BT}, \tag{3}$$

we can recast Eqs. (1) into the form

$$\frac{\partial \bar{\mathbf{x}}_n}{\partial \bar{t}} = \bar{\mathbf{x}}_{n+1} + \bar{\mathbf{x}}_{n-1} - 2\bar{\mathbf{x}}_n + \mathbf{G}_n(\bar{t}), \tag{4}$$

where

$$\bar{\mathbf{x}} = \frac{\mathbf{x}}{b}, \qquad \bar{t} = \frac{t}{\tau_1}, \tag{5}$$

are dimensionless quantities. Note that $\tau_1 = \tau_r \frac{\pi}{N^2}$, where τ_r is the Rouse relaxation time of the chain. The choice of τ_1 as unit of time leads to equations having a convenient smooth form. The components of the dimensionless random forces $G_n^i(\bar{t})$ now satisfy

$$< G_n^i(\bar{t}) >= 0, \quad < G_n^i(\bar{t}_1) G_m^j(\bar{t}_2) >= \frac{2}{3}\delta(\bar{t}_1 - \bar{t}_2)\delta_{mn}\delta_{ij},$$

For the beads adjacent to slip links from below, the evolution equations read as

$$\frac{\partial \bar{\mathbf{x}}_{N_i}}{\partial t} = \Big[-2\bar{\mathbf{x}}_{N_i} + \bar{\mathbf{x}}_{N_i-1} + \bar{\mathbf{X}}_1(\bar{t}) + \frac{l_{i+1}}{l_i}(\bar{\mathbf{X}}_i(t) - \bar{\mathbf{x}}_{N_i})\Big] + G^{\bar{x}}_{N_i}(\bar{t}), \quad i = 1, \cdots, N_{\rm seg}, \tag{6}$$

and a similar equations holds for the beads adjacent to a slip link from above. Having obtained the evolution equations of the tethered chains we now turn to their influence on the velocity of the chains in the polymer bulk that try to drag them along.

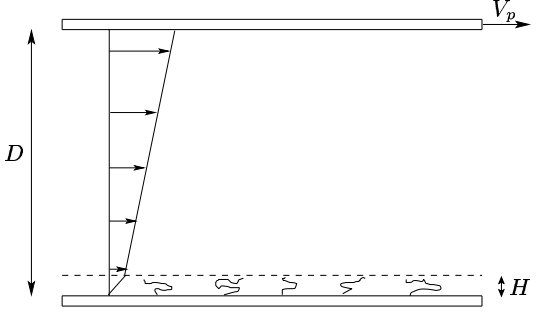

FIG. 4: Schematic representation of plane Couette flow. There are two different regions, the interfacial layer and the bulk layers. The thickness of the interfacial layer H depends on the plate velocity V_p, and is largest (of the order of the gyration radius), when the plate is not moving at all.

B. Dynamics of the bulk chains

We consider a situation as sketched in Fig. 4, which represents plane Couette flow. The upper plate is moving at a constant velocity V_p and the melt is assumed to be all the time perfectly glued to the upper plate and therefore moves with the same velocity V_p as the plate. If there is no friction between the layer adjacent to the lower plate, the velocity profile would simply be a plug profile: all layers flow with the same velocity V_p, This approximates to very good degree what has been observed experimentally for low grafting densities [9]. [28].

To show what the dynamics of the bulk chains, represented as grid points, looks like, we start from one of the simplest imaginable situations in which the polymer fluid is assumed to give rise to only three layers. Later we will generalize our discussion to an arbitrary number of layers.

1. *Three layers*

We consider the configuration as sketched in Fig. 5. Furthermore, we assume that the grafted chains can only reach the first layer and that the third layer has a velocity v_3 equal to the plate velocity V_p. The dimensionful equations for the velocities v_1 and v_2 for layers one and two are

$$\rho a \frac{dv_1}{dt} = \frac{\eta_0}{a}(v_2 - v_1) - \frac{3k_BT\nu_1}{N_e b^2}X_1$$
$$\rho a \frac{dv_2}{dt} = \frac{\eta_0}{a}(v_3 + v_1 - 2v_2). \tag{7}$$

The first equation shows that the velocity is reduced as a consequence of friction between the first and second layer and due to entanglements with the grafted chains. The density of entanglements of the grafted chains with the first layer of the bulk is denoted by ν_1. So ν_1 measures the time averaged number of slip links in the first layer that belong to the tube of a grafted chain. The

factor N_e appears in the second term of the right-hand -side of the first equation, because the equilibrium tension for a segment consisting of N_e beads is $\frac{3k_BT}{N_eb^2}$ [23]. The second equation represents that the friction between the third and second layers as well as between the second and first layer is proportional to the velocity difference between the layers and the bulk viscosity η_0 as the constant of proportionality. The viscosity η_0 is given by the expression for the viscosity for polymer melts, which means that it scales with the polymerization index Z of the bulk molecules as Z^3. In general, the chains in the bulk will be longer than the tethered chains, so $Z > N$. Since layer 2 has no interaction with grafted chains and only experiences viscous friction, the velocity of layer 2 will be equal to the average of v_1 and v_3 in the steady state.

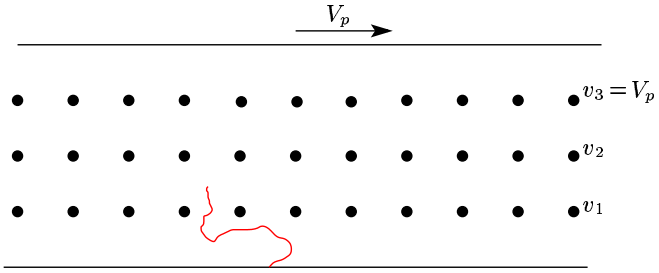

FIG. 5: Sketch of the three layered system. The plate velocity V_p is transmitted entirely to the third layer and there is only one entanglement, between the grafted chains and the first layer of the bulk molecules.

The distance between the layers is denoted by a and is equal to $\sqrt{N_e}b$ by definition [23]. The dimensionless velocities $\bar{v}_1(t)$ and $\bar{v}_2(t)$ satisfy

$$\begin{aligned} \frac{d\bar{v}_1}{d\bar{t}} &= \frac{\eta_0\tau_1}{\rho a^2}(\bar{v}_2 - \bar{v}_1) - \frac{3k_BT\tau_1^2\nu_1}{\rho N_e b^2 a}\bar{X}_1 \\ \frac{d\bar{v}_2}{d\bar{t}} &= \frac{\eta_0\tau_1}{\rho a^2}(\bar{v}_3 + \bar{v}_1 - 2\bar{v}_2) \end{aligned} \qquad (8)$$

This system of differential equations can be recast in a simple form by introducing the dimensionless parameters ϵ and θ_1. Let $\epsilon = \frac{\rho N_e b^2}{\eta_0\tau_1}$ and $\theta_1 = \frac{3k_BT\tau_1^2\nu_1}{\rho N_e^{\frac{3}{2}} b^3}$. Dropping the bars and denoting differentiation with respect to $\bar{t}$ by a dot yields a two dimensional system

$$\begin{aligned} \epsilon\dot{v}_1 &= v_2 - v_1 - \theta_1\epsilon X_1 \\ \epsilon\dot{v}_2 &= V_p + v_1 - 2v_2 \end{aligned} \qquad (9)$$

The entanglement-disentanglement transition turns out to be a matter of scales. The parameter ϵ is very small, typically of the order of $10^{-11} - 10^{-12}$, whereas θ_1 is of order $10^4 - 10^5$, at an entanglement density ν_1 equal to the critical grafting density $\nu_c = \frac{1}{R_0^2}\frac{1}{Nb^2}$. This implies that Eqs. (9) represent a singularly perturbed system. Since Eqs. (9) are linear, the system can be explicitly solved as is presented in Appendix A. Here we will make some

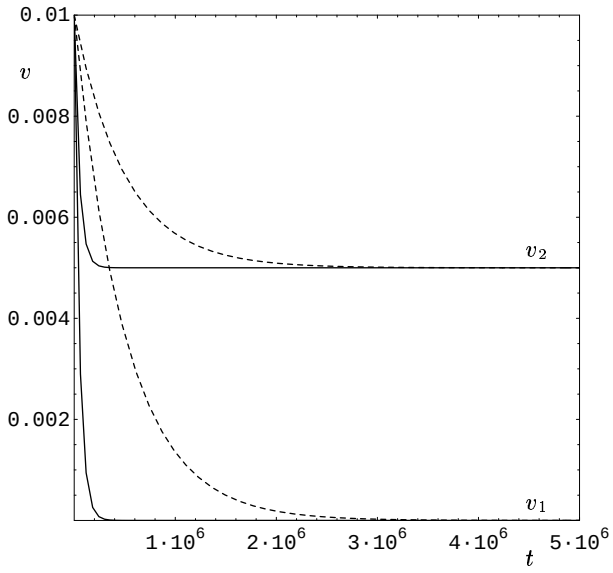

FIG. 6: The velocities v_1 and v_2 for two different values of $\epsilon\theta$. For the dashed curves $\epsilon\theta = 10^{-4}$ and the solid curves represent the case $\epsilon\theta = 10^{-6}$. In both cases $V_p = 0.01$.

qualitative remarks about the system defined by Eqs. (9) and graphically present the solution. One should notice that the parameter θ_1 is an outcome of the integration of Eqs. 4 and (7) and thus stochastic in nature. It represents the number of grafted chains interacting with the first layer of the melt. Since the chains are constantly moving and sometimes do not reach the first layer at all, θ_1 can vary between 0 and its maximal value $\theta_{\max} = \frac{3k_BT\tau_1^2\nu}{\rho N_e^{\frac{3}{2}} b^3}$. As was mentioned before, we always have $\nu > \nu_1$. The ration ν_1/ν can be interpreted as the probability for a tethered chain to reach the first layer. This probability depends on the velocity of the upper plate V_p.

There are now two extreme cases. The first case occurs when all grafted chains reach the first layer, so $\theta_1 = \theta_{\max}$. In the other extreme case all chains retract and no longer interact with the polymers in the first layer, so θ_1 vanishes. If, for illustrative purposes, θ_1 in Eq. (9) is taken constant in time and equal to $\theta_{\max}$, we find that the velocities in the first and second layer are decreasing with a typical relaxation time τ_c. The solution is shown in Fig. 6 and shows that v_2 approaches the average of v_1 and V_p, which is just $\frac{V_p}{2}$, since v_1 goes to zero and v_3 remains equal to V_p for all times. The relaxation time τ_c is given by

$$\tau_c = \frac{1}{2\theta_1\epsilon} = \frac{\eta_0 a}{6k_BT\tau_1\nu} = \frac{\eta_0\sqrt{N_e}}{2b\zeta_1\nu} \qquad (10)$$

The time-scale τ_c at which the velocity of the layers in the bulk slows down is a long time scale, due to the smallness of $\epsilon\theta_1$. It is also shown in Appendix A, that when the entanglements are released, the plug flow situation is re-

established immediately, and the entire process repeats itself from the beginning.

The slow relaxation time-scale τ_c is also present in a P-layered system. We will now write down the equations for P layers.

2. *P-layered system*

The equations of motion for a P-layered system as used in the numerical simulations are easily written down. Only the first layer and the layer in which the last segment of the tubes end obey modified equations. For all the other layers we have

$$\begin{aligned} \rho a \frac{dv_i}{dt} &= \frac{\eta_0}{a}(v_{i+1} + v_{i-1} - 2v_i) \\ &- \frac{3k_BT\nu_i(t)}{N_e b^2}(2X_i - X_{i+1} - X_{i-1}), \end{aligned} \quad (11)$$

which when expressed in dimensionless units reads

$$\begin{aligned} \frac{d\bar{v}_i}{d\bar{t}} &= \frac{\eta_0\tau_1}{\rho a^2}\left[\bar{v}_{i+1} + \bar{v}_{i-1} - 2\bar{v}_i\right] \\ &- \frac{3k_BT\tau_1^2\nu_i(\bar{t})}{\rho N_e b^2 a}\left[2\bar{X}_i - \bar{X}_{i+1} - \bar{X}_{i-1}\right]. \end{aligned} \quad (12)$$

For the first layer we have

$$\frac{d\bar{v}_1}{d\bar{t}} = \frac{\eta_0\tau_1}{a^2}\left[\bar{v}_2 - \bar{v}_1\right] - \frac{3k_BT\tau_1^2\nu_1(\bar{t})}{\rho N_e b^2 a}\left[2\bar{X}_1 - \bar{X}_2\right], \quad (13)$$

and for the $N_{\rm seg}$-th layer

$$\begin{aligned} \frac{d\bar{v}_{N_{\rm seg}}}{d\bar{t}} &= \frac{\eta_0\tau_1}{\rho N_e b^2}\left[\bar{v}_{N_{\rm seg}-1} + \bar{v}_{N_{\rm seg}+1} - 2\bar{v}_{N_{\rm seg}}\right] \\ &- \frac{3k_BT\tau_1^2\nu_{N_{\rm seg}}(\bar{t})}{\rho N_e b^2 a}\left[\bar{X}_{N_{\rm seg}} - \bar{X}_{N_{\rm seg}-1}\right]. \end{aligned} \quad (14)$$

Notice that the stochastic density of grafted chains $\nu_i(t)$ depends on i. It is well-known from the literature that on average ν_i decreases rapidly with i. The density of entanglements at a distance i from the wall relative to the grafting density ν can be interpreted as the probability that a single chain will have i entanglements with the bulk. The probability distribution of the number of entanglements i has been investigated for the case of star polymers in a number of papers [24, 25]. The time dependence of $\nu_i(t)$ is essentially the solution of a first passage problem.

We can simplify Eqs. (12-14) by introducing the same two parameters ϵ and θ_i as we did for the three layered case. We recall that ϵ is extremely small of the order of 10^{-11} and that θ_i is of order 10^5 for the lowest layer and even smaller further away from the lower plate. This means that we can rewrite Eqs. (12-14) in the form of a singularly perturbed system

$$\epsilon\frac{d\bar{v}_i}{d\bar{t}} = \left[\bar{v}_{i+1} + \bar{v}_{i-1} - 2\bar{v}_i\right] - \epsilon\theta_i\left[2\bar{X}_i - \bar{X}_{i+1} - \bar{X}_{i-1}\right]. \quad (15)$$

The equations for the first and $N_{\rm seg}$-th layer are changed accordingly. In our numerical simulations we integrate the system of Eqs. (15), while at the mean time integrating the stochastic differential equations of the chain within the tube (4) and (7). One should note that the coupling between Eqs. (4) and (7) on the one hand and Eq. (15) on the other hand is established via the stochastic parameter θ_i, which measures the local and temporary entanglements between bulk layers and grafted chains.

III. SIMULATION RESULTS

We performed numerical simulations on the system defined by Eqs. (4), (7) and (15). Where possible, the parameter values were taken in accordance with Ref. [9], in which experiments performed on a PDMS melt are described. We consider a configuration in which the distance D between the two plates is 10μ m. The typical length of a Kuhn segment is $b = 10$Å. We further take the number of monomers of a chain attached to the wall N fixed and equal to 100 in order to be able to do calculations within a reasonable time span. The entanglement length N_e is set equal to 10, unless mentioned otherwise. The temperature T is of the order of $300K$, which implies a time τ_1 of the order of μs, which is in agreement with Ref. [26]. The parameter $\theta_{\max}\epsilon$ will be varied between 10^{-4} and 10^{-7} which corresponds to changing the grafting density from $\nu = 0.1\nu_c$ to 100 times the critical density ν_c.

In Fig. 7 a logarithmic plot of the dimensionless slip velocity $\bar{V}_s$ is presented as a function of the (dimensionless) plate velocity $\bar{V}_p$. It displays the three slip velocity regimes that were expected. For small $\bar{V}_p$ the slope of the curve is constant. The value of $\bar{V}_p$ for which the slope starts to increase is denoted by $\bar{V}_p^\star$. For $\bar{V}_p > \bar{V}_p^\star$ the slope has initially a higher value. This region is referred to as the transition region. For very large values of $\bar{V}_p$ the slope approaches one. The transition is only mild and not very sharp in contrast with the predictions in Ref. [3]. From experiments it is known [9], that the transition depends on the density of the grafted chains and the number of entanglements. In fact, for densities $\nu \approx \nu_c$, no sharp transition is observed, but only a mild transition comparable to ours [9]. Only when the densities are increased well beyond ν_c, say 10 to 100 times ν_c, the transition is very sharp, almost vertical.

The data of Fig. 7 can also be presented by looking at the so-called extrapolation length l, defined by $l = \frac{V_s D}{V_p - V_s}$. We see from Fig. 8, that the l/D versus $\bar{V}_{\rm slip}$ curve exhibits a crossover from practically constant to approximately linearly increasing. The crossover in the velocity and l/D was also observed in the experiments in Refs. [7] and [9] and were predicted by de Gennes in Ref. [3].

To find the dependence on the number of entanglements we performed simulations with $N_e = 5$. The results of these are depicted in Fig. 9. It shows that

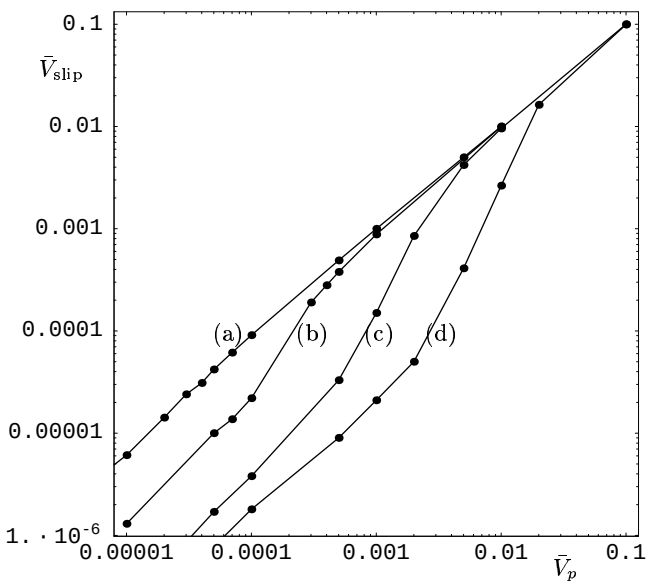

FIG. 7: Slip velocity as a function of the upper plate velocity $\bar{V}_p$ for $\epsilon\theta_{\rm max} = 10^{-7}$ (a), $\epsilon\theta_{\rm max} = 10^{-6}$ (b), $\epsilon\theta_{\rm max} = 10^{-5}$ (c), and $\epsilon\theta_{\rm max} = 10^{-4}$ (d). The beginning of the transition region increases with increasing $\epsilon\theta_{\rm max}$ in agreement with experiment and the predictions in Ref. [3]. Also the transition is more pronounced for larger values of $\epsilon\theta_{\rm max}$, which has also been observed experimentally.

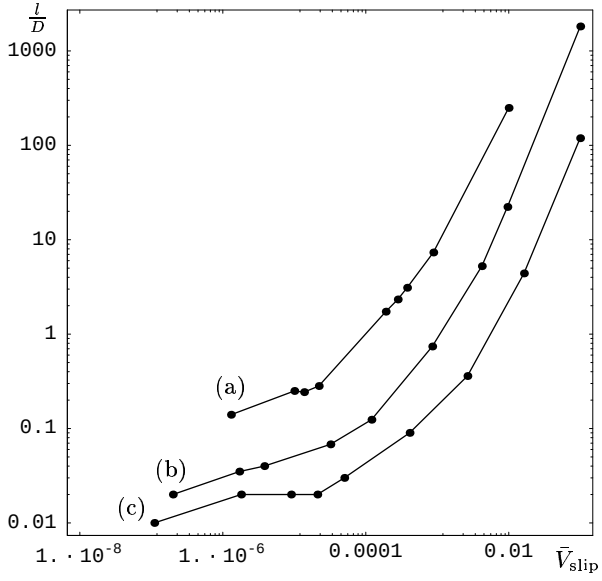

FIG. 8: The extraplation length l/D as a function of the slip velocity $\bar{V}_{\rm slip}$ for three different values of $\epsilon\theta_{\rm max}$. Curve (a) corresponds to $\epsilon\theta_{\rm max} = 10^{-6}$, (b) to $\epsilon\theta_{\rm max} = 10^{-5}$, and (c) to $\epsilon\theta_{\rm max} = 10^{-4}$. The sudden increase of $\bar{V}_{\rm slip}$ is most clearly present for $\epsilon\theta_{\rm max} = 10^{-4}$, which has the largest grafting density.

the transition becomes sharper with decreasing N_e values which corresponds to enhancement of the number of entanglements. From the simulations it can be inferred that at $\bar{V}_p = \bar{V}_p^\star$ the relaxation mechanism for the tethered chains has changed. In fact, $V_p^\star$ designates the value of the plate velocity above which CCR is the dominating relaxation mechanism of the tethered chains. For plate velocities smaller than $\bar{V}_p^\star$, the bulk flow is slowed down so much that the constraints are no longer removed from the tethered chain by CCR and therefore the other relaxation mechanism, arm retraction, becomes dominant.

Considering the grafted chain conformations and the velocity profile of the grid elucidates the processes that take place if one increases the plate velocity. In Fig. 10 two chain conformations and two velocity profiles are depicted for two different values of $\bar{V}_p$. Chain (a) corresponds to $\bar{V}_p = 0.005$ and (b) to $\bar{V}_p = 0.001$. Since the bulk flow tries to drag the grafted chains along, they will always be partially parallel to the wall. This part of the chain will be longer for higher $\bar{V}_p$, which agrees with Fig. 10. The tail of the chain can escape the dragging of the grid by arm retraction and subsequently tube renewal or breathing. Precisely this process is displayed in Fig. 10. Since the drag is stronger for higher values of $\bar{V}_p$, chain (a) has a smaller tail which point upwards than chain (b). The consequences for the velocity profile are that there is less slowing down for chain (a) than for chain (b), since there are fewer entanglements for (a) than for (b). Also the velocity profile for (b) shows that the velocity decreases faster closer to the wall.

Another important quantity is the shear stress. The shear stress can be calculated by using the Kirkwood expression for the stress, which in the case of the tube model reduces to [23].

$$\sigma_{xy}^{\rm entang}(t) = \frac{3ck_BT}{Nb^2}\left\langle \int_0^L dsL(t)u_x(s,t)u_y(s,t)\right\rangle, \quad (16)$$

where c is the number of polymers per unit volume, L the length of the tube and $u_x(s,t), u_y(s,t)$ denote the x and y components of the vector tangent at the tube at position s at time t. The contour length coordinate s is zero at the wall and L at the end of the tube. There is another contribution to the stress besides the one given in Eq. (16). At high plate velocities the grafted chains are dragged along with the flow and orient parallel to the wall. Nevertheless, they experience friction due to the bulk chains that flow along, although there are no entanglements. Under entanglement conditions the stress contribution due to the friction with the bulk chains, is negligible compared to the stress associated with the entanglements. However, when there are hardly any entanglements left, due to the high plate velocities, the contribution from the friction between the first bulk layer and horizontally oriented grafted chain, called Rouse-friction, is dominant. From physical arguments its is easily seen that the stress $\sigma^{\rm Rouse}$ corresponding to Rouse-friction is

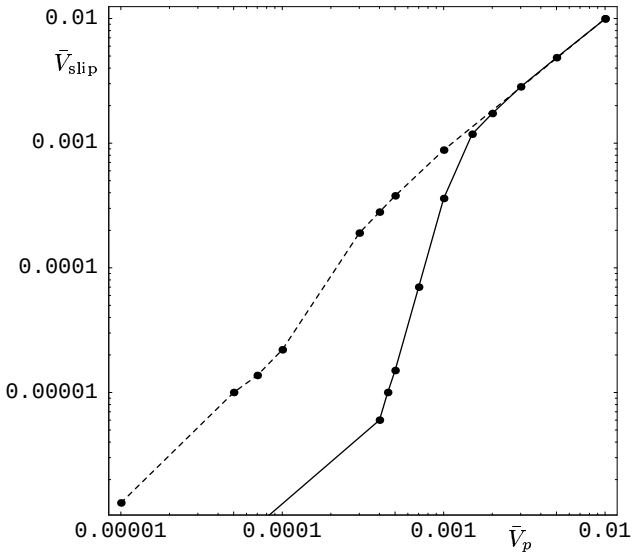

FIG. 9: Slip velocity as a function of the upper plate velocity $\bar{V}_p$ for $\epsilon\theta_{\max} = 10^{-6}$, but for different values of N_e. The dashed curve corresponds to $N_e = 10$ and the solid one to $N_e = 10$. The transition for $N_e = 5$ is much steeper than for $N_e = 10$.

given by

$$\sigma_{xy}^{\rm Rouse} = \zeta\nu\frac{N}{N_e}V_{\rm slip}. \tag{17}$$

Here ζ is equal to the monomer friction ζ_1 if one assumes that the interaction between the wall and the monomers is equally strong. If this is not the case one needs an expression for ζ which takes into account the characteristics of the wall. Since here we focus on the entanglement-disentanglement transition, we will simply take $\zeta = \zeta_1$. If we add the two stress contributions, we obtain that the total shear stress $\sigma_{xy}^{\rm tot}$ is

$$\sigma_{xy}^{\rm tot} = \frac{3ck_BT}{Nb^2}\left\langle\int_0^L dsL(t)u_x(s,t)u_y(s,t)\right\rangle + \zeta_1\frac{N}{N_e}V_{\rm slip}. \tag{18}$$

In dimensionless units the shear stress $\bar{\sigma}_{xy}^{\rm tot}$ becomes

$$\bar{\sigma}_{xy}^{\rm tot} = \frac{\sigma_{xy}^{\rm tot}b}{3k_BT\nu_c} = \nu_r\left[\sum_{i=1}^{N_{\rm seg}}\left\langle\frac{u_x(i)u_y(i)L_{\rm seg}^2(i)}{NN_e}\right\rangle + \bar{V}_{\rm slip}\frac{N}{N_e}\right] \tag{19}$$

Here ν_r is the grafting density relative to the critical grafting density ν_c, $N_{\rm seg}$ measures the number of tube segments and $L_{\rm seg}(i)$ is the length of the i-th tube segment. This is clarified in Fig. 11. When the chain is aligned with the wall, the first term vanishes and we are left with a term increasing linearly with $V_{\rm slip}$. The expression we used for the stress is similar to the one used

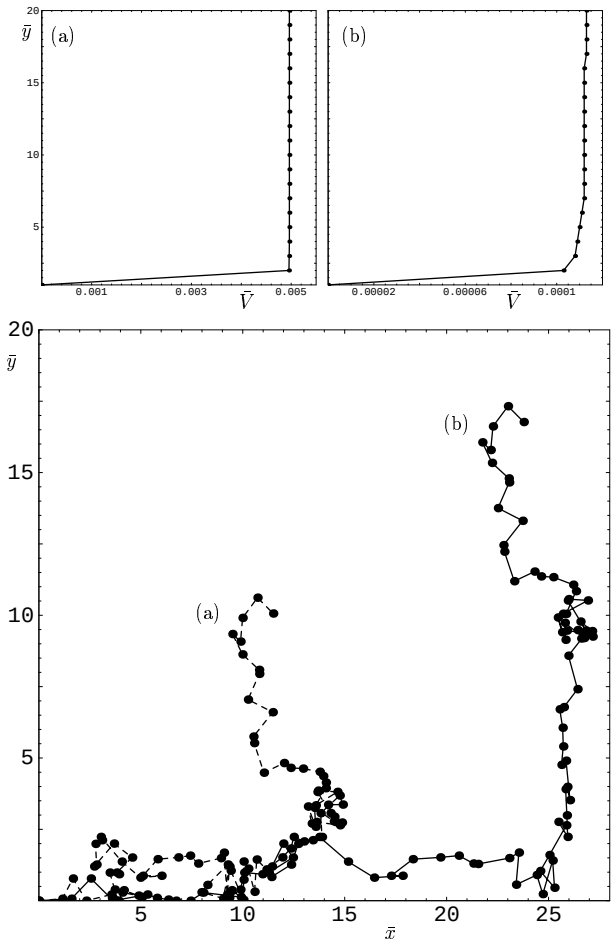

FIG. 10: Two chain conformations and velocity profiles for two different values of $\bar{V}_p$ and with $\epsilon\theta_{\max} = 10^{-6}$ and $N_e = 5$. Configuration (a) corresponds to $\bar{V}_p = 0.005$ and (b) represents $\bar{V}_p = 0.001$. The chains both have a part which is approximately horizontal and a tail that is entangled with the bulk which points upwards. The velocity profile (a) corresponds nearly to plug flow, since the interfacial layer is very small. The velocity profile (b) reveals that the velocity tends to zero over an interfacial layer consisting of a few bulk layers.

in Ref. [12]. In Ref. [3] the dimensionless stress $\bar{\sigma}_{xy}^L$ apart from the Rouse contribution was defined by

$$\bar{\sigma}_{xy}^L = \frac{\sigma_{xy}^L b}{3k_BT\nu_c} = \nu_r\frac{\bar{L}}{N}, \tag{20}$$

which is proportional to the length of the tethered chain.

In Fig. 12 the stresses according to the two definitions above are shown for $N_e = 5$. The chain length and stress are seen to exhibit the same behavior. There is a maximum at the same value of $\bar{V}_p$, but the maximum occurs at $\bar{V}_p = 0.005$, whereas the transition region starts at $\bar{V}_p = \bar{V}_p^\star = 0.0005$. The fact that the maximum in the stress is attained at values of $\bar{V}_p \gg \bar{V}_p^\star$ can be explained as

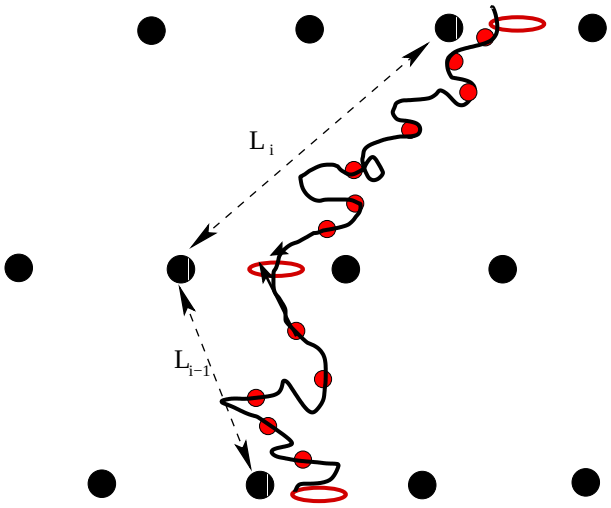

FIG. 11: Schematic representation of a tube segement to illustrate the meaning of length of tube segment i in Eq. (21), which defines the shear stress. L_i is the distance between two gridpoints, or equivalently slip links, through which the chain passes.

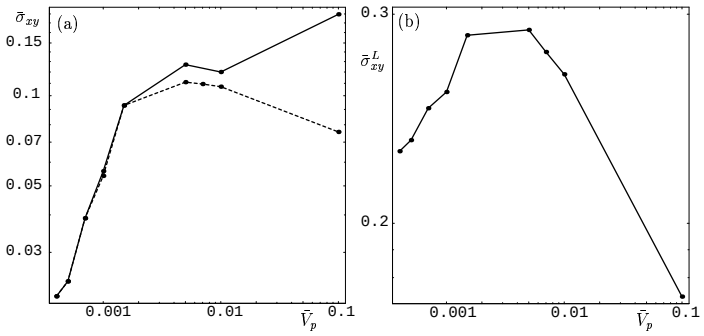

FIG. 12: In (a) the stress, as defined by Eq. (21), is shown as a function of the plate velocity $\bar{V}_p$. It clearly shows that it attains a maximal value for $\bar{V}_p = 0.005$, which is well beyond the value of $\bar{V}_p$ at the onset of slip $\bar{V}_p^\star = 0.0005$. The dashed line represents the stress contribution due to the entanglements, the solid line is the total stress which includes the Rouse friction part, which becomes dominant as $\bar{V}_p$ is large. In (b) the dimensionless stress as defined by Eq. (20), is plotted and it shows a maximum for the same value of $\bar{V}_p$ as σ_{xy}^{tot}.

follows. If $\bar{V}_p$ is gradually increased the stress increases, since the tethered chains will start to orientate in the flow. Increasing the plate velocity beyond $V_p^\star$, does not really change this. The molecule is stretched, but still feels the constraints and therefore the stress continues to increase with $\bar{V}_p$. When $\bar{V}_p$ is sufficiently large to push the tethered parallel to the wall the stress due to entanglements starts to decrease steeply. At the same time the Rouse-stress begins to grow linearly with $\bar{V}_p$. This results in an S-shaped stress versus velocity curve, which may give rise to instabilities like spurt.

IV. CONCLUSIONS AND DISCUSSION

We proposed a self-consistent model to explain wall slip from a molecular point of view. The model contains two important relaxation mechanisms for grafted chains: CCR and arm retraction. It was demonstrated that when the model was applied in a plane Couette-flow geometry from low to moderate grafting densities, it indeed exhibits a stick-slip transition in agreement with experiments. This can be explained as a transition from arm retraction to CCR as the dominating relaxation mechanism for the tethered chain. The velocity profile was also calculated and shown to display volatile behavior on short time scales and to be slowly decaying on much longer time scales. From analytical calculations for a simple three layered system, the time scale determining the velocity decay could be identified. It turned out that the time scale at which the melt is slowed down compared to the relaxation time of the tethered chain is the quintessential quantity behind the stick-slip mechanism.

The stress was also calculated and it was demonstrated that the stress exhibits a maximum as a function of the the plate velocity. The maximum is attained at a value of $\bar{V}_p$ which does not coincide with $\bar{V}_p^\star$, but is much larger. This is due to the fact that only for such large plate velocities the bulk chains succeed in pushing the tethered chains parallel to the wall.

In our analysis we have made some crucial assumptions. First we assumed that the surface at which the chains are tethered is smooth, which is not the case in practice. We think, that a rough surface would eventually be smoothened as the cavities will be filled with polymers. However, if a chain near the wall entangles with the chains residing in the cavities, it would not be really grafted on the wall, but entangled with a coil of polymers in a cavity. In this case links between bulk chains might actually be stronger than the links between the chain and the polymers in the cavity. This suggests that for rough surfaces the bonding-debonding mechanism should also be considered.

Furthermore, in order for our model to be applicable in practice it is necessary to deal with polydispersity. This implies that one has to average over a distribution of chains lengths. If the numerics can be improved upon it is in principle feasible to perform numerical simulations for different chain lengths and obtain slip velocity and stress as averages of these simulations.

So far, we were only able to numerically integrate the evolution equations of the dynamical system. We are currently investigating analytical approximations, which

would allow us to give estimate of how the beginning of the transition region and the velocity of which the stress maximum is attained, depend on the molecular parameters.

We further remark that the effect of loops is neglected. This can be justified, since it is far harder for a loop to relax completely and therefore they do not contribute to jumps in the velocity, but rather give an overall slowing down of velocity of the fluid. Such an effect could also be incorporated by putting it in the effective relaxation time of the tethered chains.

The model we considered is only two-dimensional. Extension to three dimensions is another refinement, which we would like to include. This would probably have a small effect on the θ_i parameter, but it is not expected to lead to any qualitatively different results, since the entanglement mechanism remains the same.

There are many possible applications of the proposed model, since the agreement between experiment and predictions is good and generalization to polydisperse system seems to be tractable. It may, for example, be applied in the prediction of spurt, which requires a known slip wall. To extract such a slip wall from the model and combine them with a constitutive equation to make predictions for spurt is a challenge for future investigations.

V. APPENDIX A

One can rewrite Eqs. (9) after another differentiation in the matrix form

$$\begin{pmatrix} \dot{x} \\ \dot{y} \\ \dot{z} \end{pmatrix} = \begin{pmatrix} 0 & 1 & 0 \\ 0 & 0 & 1 \\ -\frac{2\theta}{\epsilon} & \frac{-1-\theta\epsilon^2}{\epsilon^2} & -\frac{3}{\epsilon} \end{pmatrix} \begin{pmatrix} x \\ y \\ z \end{pmatrix}$$

where x, y, z now stand for $v_1, \dot{v}_1, \ddot{v}_1$, respectively. The corresponding eigenvalue equation reads as

$$\lambda^3 + \frac{3\lambda^2}{\epsilon} + \lambda\left[\frac{1+\theta\epsilon^2}{\epsilon^2}\right] + \frac{2\theta}{\epsilon} = 0. \tag{21}$$

This third order equation is easily solved and yields the following three negative eigenvalues

$$\begin{aligned} \lambda_1 &= -\frac{1}{\epsilon}\left[1 + 2\sqrt{\frac{2-\theta\epsilon^2}{3}}\cos\left(\frac{\phi}{3}\right)\right], \\ \lambda_2 &= -\frac{1}{\epsilon}\left[1 + 2\sqrt{\frac{2-\theta\epsilon^2}{3}}\cos\left(\frac{\phi}{3} + \frac{2\pi}{3}\right)\right], \\ \lambda_3 &= -\frac{1}{\epsilon}\left[1 + 2\sqrt{\frac{2-\theta\epsilon^2}{3}}\cos\left(\frac{\phi}{3} - \frac{2\pi}{3}\right)\right]. \end{aligned} \tag{22}$$

Here ϕ is defined by

$$\phi = \arccos\left[-\sqrt{\frac{27(1+\theta\epsilon^2)^2}{4(2-\theta\epsilon^2)^3}}\right]. \tag{23}$$

Eqs. (23) are, to an excellent approximation, equal to

$$\begin{aligned} \lambda_1 &= -\frac{\theta\epsilon}{2}\sqrt{\frac{2}{3}}\cos\left(\frac{1}{3}\arccos\left[-\sqrt{\frac{27}{32}}\right]\right) \\ &= -2\theta\epsilon \\ \lambda_2 &= -\frac{1}{\epsilon}\left[1 + 2\sqrt{\frac{2}{3}}\cos\left(\frac{1}{3}\arccos\left[-\sqrt{\frac{27}{32}}\right] + \frac{2\pi}{3}\right)\right] \\ &= -\frac{3-\sqrt{5}}{2\epsilon} \\ \lambda_3 &= -\frac{1}{\epsilon}\left[1 + 2\sqrt{\frac{2}{3}}\cos\left(\frac{1}{3}\arccos\left[-\sqrt{\frac{27}{32}}\right] + \frac{2\pi}{3}\right)\right] \\ &= -\frac{3+\sqrt{5}}{2\epsilon} \end{aligned} \tag{24}$$

We can now write down the solution for $v_1(t)$ by imposing the initial conditions $v_1(0) = V_p$, $\dot{v}_1(0) = -\theta X_1(0)$, $\ddot{v}_1(0) = \frac{\theta X_1(0)}{\epsilon} - V_p\theta$, which yields

$$v_1(t) = C_1 e^{\lambda_1 t} + C_2 e^{\lambda_2 t} + C_3 e^{\lambda_3 t}, \tag{25}$$

where C_1, C_2, C_3 are functions of the eigenvalues and the initial values and given by

$$\begin{aligned} C_1 &= -\frac{\theta - \epsilon V_p - \epsilon\lambda_2\lambda_3 V_p - \epsilon\lambda_2\theta X_1(0) - \epsilon\lambda_3\theta X_1(0)}{\epsilon(\lambda_1-\lambda_2)(\lambda_1-\lambda_3)} \\ C_2 &= -\frac{-\theta + \epsilon V_p - \epsilon\lambda_1\lambda_3 V_p + \epsilon\lambda_1\theta X_1(0) + \epsilon\lambda_3\theta X_1(0)}{\epsilon(\lambda_1-\lambda_2)(\lambda_2-\lambda_3)} \\ C_3 &= -\frac{-\theta - \epsilon V_p - \epsilon\lambda_1\lambda_2 V_p - \epsilon\lambda_1\theta X_1(0) - \epsilon\lambda_2\theta X_1(0)}{\epsilon(\lambda_1\lambda_2 - \lambda_1\lambda_3 - \lambda_2\lambda_3 + \lambda_3^2)}. \end{aligned}$$

One can easily see that C_1 is of the order of V_p, up to an order ϵ correction, so that $v_2(t) - v_1(t)$ is almost equal to $V_p - v_2(t)$, which shows that the shear rate is homogeneous throughout the flow. The velocity of the first layer slows down to zero exponentially with a typical relaxation rate of $2\theta\epsilon$. The second layer is slowed down at the same rate to $\frac{V_p}{2}$

$$\begin{aligned} v_2(t) &= \frac{V_p}{2}\left[1 + e^{-\frac{2}{\epsilon}t}\right] + C_1\left[\frac{e^{\lambda_1 t} - e^{-\frac{2}{\epsilon}t}}{2+\lambda_1\epsilon}\right] \\ &+ C_2\left[\frac{e^{\lambda_2 t} - e^{-\frac{2}{\epsilon}t}}{2+\lambda_2\epsilon}\right] + C_3\left[\frac{e^{\lambda_3 t} - e^{-\frac{2}{\epsilon}t}}{2+\lambda_3\epsilon}\right]. \end{aligned} \tag{26}$$

The important convective relaxation time τ_c is given by

$$\tau_c = \frac{1}{2\theta\epsilon} = \frac{\eta_0\sqrt{N_e}b}{6k_BT\tau_1\nu} = \frac{\eta_0\sqrt{N_e}}{2b\zeta_1\nu}. \tag{27}$$

The case $\theta = 0$ is simplest since then Eqs. (9) reduce to

$$\begin{aligned} \epsilon\dot{v}_1 + v_1 &= v_2 \\ \epsilon\dot{v}_2 + 2v_2 &= v_3 + v_1. \end{aligned} \tag{28}$$

Solving for v_1 gives the following expression for $v_1(t)$

$$v_1(t) = V_p e^{-\frac{t}{\epsilon}} + \frac{e^{-\frac{t}{\epsilon}}}{\epsilon} \int_0^t e^{\frac{t'}{\epsilon}} v_2(t')\, dt'. \qquad (29)$$

When Eq. (29) is substituted in the evolution equation for v_2, we obtain after differentiating one more time the differential equation for $v_2(t)$

$$\epsilon \ddot{v}_2 + 3\dot{v}_2 + \frac{v_2}{\epsilon} = \frac{V_p}{\epsilon}, \qquad (30)$$

which is readily solved and gives

$$v_2(t) = V_p + A \exp\left[-\frac{3+\sqrt{5}}{2\epsilon}t\right] + B \exp\left[-\frac{3-\sqrt{5}}{2\epsilon}t\right]. \qquad (31)$$

The coefficients A and B are determined by V_p and the value of the velocity in the first and second layer just before θ becomes zero, $v_1(0)$ and $v_2(0)$ respectively, as follows

$$A = \frac{v_2(0)(1+\sqrt{5}) + V_p(1-\sqrt{5}) - 2v_1(0)}{2\sqrt{5}},$$

$$B = \frac{v_2(0)(-1+\sqrt{5}) - V_p(1+\sqrt{5}) + 2v_1(0)}{2\sqrt{5}}.$$

For v_1 we have a similar expression as for v_2

$$\begin{aligned} v_1(t) &= V_p + \left[\frac{2A}{1+\sqrt{5}} - \frac{2B}{-1+\sqrt{5}}\right] \exp\left[-\frac{t}{\epsilon}\right] \\ &- \frac{2A}{1+\sqrt{5}} \exp\left[-\frac{3+\sqrt{5}}{2\epsilon}t\right] \\ &+ \frac{2B}{-1+\sqrt{5}} \exp\left[-\frac{3-\sqrt{5}}{2\epsilon}t\right]. \end{aligned} \qquad (32)$$

Eqs. (31) and (32) show that the velocity profile jumps, almost instantaneously, back to the initial plug profile.

[1] M. Sun and C. Ebner, Phys. Rev. Lett. **69**, 3491 (1992).
[2] M. Mooney, J. Rheol. **2**, 210, (1931).
[3] P.G. de Gennes, C.R. Acad. Sc. Paris, Serie B **288** 219 (1979).
[4] F. Brochard and P.G. de Gennes, Langmuir **8**, 3033 (1992).
[5] F. Brochard-Wyart, C. Gay, and P.G. de Gennes, Macromolecules **29**, 377 (1996).
[6] A. Adjari, F. Brochard-Wyart, P.G. de Gennes, L. Leibler, J.L. Viovy, M. Rubinstein, Physica A **204**, 17 (1994).
[7] K.B. Migler, H. Hervet, and L. Léger, Phys. Rev. Lett. **70**, 287 (1993).
[8] K.B. Migler, G. Massey, H Hervet, and L. Léger, J. Phys. Condens. Matter **6**, A301-304 (1994).
[9] L. Léger, H. Hervet, G. Massey, and E. Durliat, J. Phys. Condens. Matter, **9**, 7719 (1997).
[10] J.D. Shore, D. Ronis, L. Piché, and M. Grant, Phys. Rev. E **55**, 2976 (1997).
[11] J.D. Shore, D. Ronis, L. Piché, and M. Grant, Phys. Rev. Lett. **77**, 655 (1996).
[12] Y. M. Joshi, A.L. Lele, and R.A. Mashelkar, Macromolecules, **34**, 3412 (2001).
[13] D.W. Mead, R.G. Larson, and M. Doi, Macromolecules **31**, 7895 (1998).
[14] C.C. Hua, J. D. Schieber, J. Chem. Phys. **109**, 10018 (1998)
[15] P.P. Dra and S.Q. Wang, Phys. Rev. Lett. **75**, 2698 (1995).
[16] Y.I. Inn and S.Q. Wang, Phys. Rev. Lett. **76**, 467 (1996).
[17] M.M. Denn, Ann. Rev. Fluid. Mech. **22**, 13 (1990).
[18] M.M Denn, Annu. Rev. Fluid. Mech. **33**, 265 (2001).
[19] S.G. Hatzikiriakos and J.M. Dealy, J. Rheol. **36**, 845 (1992).
[20] M. Doi and S.F. Edwards, J.C.S. Faraday II **74**, 1789 (1978).
[21] M. Doi and S.F. Edwards, J.C.S. Faraday II **74**, 1802 (1978).
[22] M. Doi and S.F. Edwards, J.C.S. Faraday II **75**, 38 (1978).
[23] M. Doi and S.F. Edwards, *The theory of polymer dynamics*, Oxford Science Publications (1986).
[24] D.S. Pearson, E. Helfland, Macromolecules **17**, 888 (1984).
[25] R.C. Ball and T.C.B. McLeish, Macromolecules **22**, 1911 (1989).
[26] A.L. Yarin, M.D. Graham, J. Rheol. **42**, 1491 (1998).
[27] The instantaneous stress is oscillating, reaching a maximum when the tethered and bulk chains are maximally entangled and a minimum when the entanglements are released.
[28] If one supposes that there is equal slip at the upper and lower plate, this will lead to a factor of two in the slip velocity, but does not lead to any qualitative changes.